

A Deuterium NMR Spectroscopic Study of Solid BH_3NH_3

Glenn H. Penner,* Y. C. Phillis Chang, and Jennifer Hutzal

Department of Chemistry and Biochemistry, University of Guelph, Guelph, Ontario, Canada N1G 2W1

Received December 1, 1998

Deuterium nuclear magnetic resonance (NMR) powder spectra and spin–lattice relaxation times (T_1) are used to measure the deuterium quadrupolar coupling constants (QCCs) $\chi(\text{BD})$ and $\chi(\text{ND})$ and to investigate the molecular reorientation of the BD_3 and ND_3 groups in solid deuterated borane monoammoniate, BD_3NH_3 and BH_3ND_3 , respectively. In the high-temperature, tetragonal, phase (above 225 K) the following Arrhenius parameters are obtained from the temperature-dependent T_1 : $E_a = 5.9 \pm 0.5$ kJ/mol and $\tau_\infty = 1.1 \times 10^{-13}$ s for BD_3NH_3 ; $E_a = 7.3 \pm 0.8$ kJ/mol and $\tau_\infty = 4.4 \times 10^{-14}$ s for BH_3ND_3 . In the low-temperature, orthorhombic, phase the following parameters are obtained: $E_a = 26.4 \pm 1.4$ kJ/mol and $\tau_\infty = 1.2 \times 10^{-17}$ s for BD_3NH_3 ; $E_a = 13.7 \pm 0.9$ kJ/mol and $\tau_\infty = 5.7 \times 10^{-15}$ s for BH_3ND_3 . Here τ_∞ is proportional to the inverse of the usual Arrhenius preexponential factor, A . Deuterium line shape measurements for the low-temperature phase of BD_3NH_3 yield $E_a = 25 \pm 2$ kJ/mol and $\tau_\infty = 4.7 \times 10^{-19}$ s. These dynamic factors indicate that the molecule is probably undergoing whole molecule rotation above the phase transition but the BH_3 and NH_3 groups are undergoing uncorrelated motion in the low-temperature phase. Deuterium quadrupolar coupling constants of 105 ± 10 and 200 ± 10 kHz were determined for BD_3NH_3 and BH_3ND_3 , respectively. Molecular orbital (MO) calculations (CI(SD)/6-31G(d,p)//MP2/6-31G(d,p)) for the isolated molecule yield values of 143 and 255 kHz. MO calculations also show that the deuterium quadrupolar coupling constants $\chi(\text{BD})$ and $\chi(\text{ND})$ are relatively insensitive to all molecular structural parameters except the B–H and N–H bond lengths, respectively. It is suggested that the large decrease in the QCC on going from the gas phase to the solid state may be due to a slight lengthening of the B–H and N–H bonds, possibly a result of attractive B–H \cdots H–N interactions.

Introduction

Since BH_3NH_3 , borane monoammoniate, was first synthesized and isolated by Shore and Parry,^{1,2} its physical properties have been investigated by many workers. The microwave spectra of nine isotopomers of BH_3NH_3 have been measured and yield the gas-phase geometry, dipole moment, and barrier to internal rotation.^{3,4} A more recent, high resolution, spectrum provided gas-phase values of the ^{11}B (^{10}B) and ^{14}N nuclear quadrupolar coupling constants (QCCs).⁵

Several X-ray diffraction derived crystal structures of powder samples have been reported.^{6–8} The nuclear QCC values have been determined for ^{11}B and ^{14}N in solid BH_3NH_3 .⁹ A thorough ^1H and ^{11}B T_1 and $T_{1\rho}$ study of solid BH_3NH_3 has been undertaken and provides insight into the crystal structure and dynamics of the BH_3NH_3 molecule in the two solid phases.¹⁰ There have been numerous theoretical investigations of the molecular structure and physical properties of BH_3NH_3 , including geometry,^{11–20} dipole moment,^{20–22} electric fields, electric

field gradients, diamagnetic shielding and susceptibility,²¹ B–N bond dissociation energy,^{15–18} torsional barrier,^{14,20} and vibrational frequencies.²² In solution, the dipole moment has been measured²³ and the vibrational modes have been assigned.²⁴ The ^{11}B , ^{14}N , ^{15}N , and ^1H chemical shifts and spin–spin coupling constants have been measured in a number of solvents.^{25–30} The ^{11}B , ^{10}B , and ^{14}N spin–lattice relaxation times (T_1) have been measured in aqueous solution and related to the nuclear QCCs as obtained by microwave spectroscopy, nuclear quadrupolar resonance (NQR) spectroscopy, and ab initio molecular orbital theory.³¹

- (1) Shore, S. G.; Parry, R. W. *J. Am. Chem. Soc.* **1955**, *77*, 6084.
- (2) Shore, S. G.; Parry, R. W. *J. Am. Chem. Soc.* **1958**, *80*, 8.
- (3) Suenram, R. D.; Thorne, L. R. *Chem. Phys. Lett.* **1981**, *78*, 157.
- (4) Thorne, L. R.; Suenrum, R. D.; Lovas, F. J. *J. Chem. Phys.* **1983**, *78*, 167.
- (5) Vorman, K.; Dreizler, H. Z. *Naturforsch., A* **1991**, *46*, 1060.
- (6) Hughes, E. W. *J. Am. Chem. Soc.* **1956**, *78*, 506.
- (7) Lippert, E. L.; Lipscomb, W. N. *J. Am. Chem. Soc.* **1956**, *78*, 503.
- (8) Hoon, C. F.; Reynhardt, E. C. *J. Phys. C* **1983**, *16*, 6129.
- (9) Lötzer, A.; Voitländer, J. *J. Magn. Reson.* **1982**, *48*, 1.
- (10) Reynhardt, E. C.; Hoon, C. F. *J. Phys. C* **1983**, *16*, 6137.
- (11) Armstrong, D. R.; Perkins, P. G. *Inorg. Chim. Acta* **1974**, *10*, 77.
- (12) Peyerimhoff, S. D.; Buenker, J. J. *Chem. Phys.* **1968**, *49*, 312.
- (13) Veillard, A. *Chem. Phys. Lett.* **1969**, *3*, 128.
- (14) Umeyama, H.; Morokuma, K. *J. Am. Chem. Soc.* **1976**, *98*, 7208.

- (15) Zirz, C.; Ahlrichs, R. *J. Chem. Phys.* **1981**, *75*, 4980.
- (16) Ahlrichs, R.; Koch, W. *Chem. Phys. Lett.* **1978**, *53*, 341.
- (17) Redman, L. T.; Purvis, G. D.; Bartlett, R. J. *J. Am. Chem. Soc.* **1979**, *101*, 2856.
- (18) Anane, H.; Boutalib, A.; Nebat-Gil, I.; Tomas, F. J. *Phys. Chem. A* **1998**, *102*, 7070.
- (19) Dill, J. D.; Schleyer, P. v. R.; Pople, J. A. *J. Am. Chem. Soc.* **1975**, *97*, 3402.
- (20) Binkley, J. S.; Thorne, L. R. *J. Chem. Phys.* **1983**, *79*, 2932.
- (21) Dixon, M.; Palke, W. E. *J. Chem. Phys.* **1974**, *61*, 2250.
- (22) Brint, P.; Sangchakr, B.; Fowler, P. W. *J. Chem. Soc., Faraday Trans. 2* **1989**, *85*, 29.
- (23) Weaver, J. R.; Shore, S. G.; Parry, R. W. *J. Chem. Phys.* **1958**, *29*, 1.
- (24) Smith, J.; Seshadri, K. S.; White, D. J. *Mol. Spectrosc.* **1993**, *15*, 327.
- (25) Gaines, D. F.; Schaeffer, R. J. *J. Am. Chem. Soc.* **1964**, *86*, 1505.
- (26) Schaeffer, R.; Tebbe, F.; Phillips, C. *Inorg. Chem.* **1964**, *3*, 1475.
- (27) Heitsch, C. W. *Inorg. Chem.* **1965**, *4*, 1019.
- (28) Nöth, H.; Wrackmeyer, B. *Chem. Ber.* **1974**, *109*, 3070.
- (29) Hu, M. G.; Van Paaschen, J. M.; Geanangel, R. A. *J. Inorg. Nucl. Chem.* **1977**, *34*, 2147.
- (30) Wrackmeyer, B. *J. Magn. Reson.* **1986**, *66*, 172.
- (31) Penner, G. H.; Daleman, S. I.; Custodio, A. R. *Can. J. Chem.* **1992**, *70*, 2420.
- (32) Bühl, M.; Steinke, T.; Schleyer, P. v. R.; Boese, R. *Angew. Chem., Int. Ed. Engl.* **1991**, *30*, 1160.

There are two interesting and unusual properties of BH₃NH₃. First, BH₃NH₃ is a solid at room temperature, and second, the B–N bond length appears to differ significantly (by ca. 0.1 Å) between the gas and solid phases.³² Crabtree et al.^{33,34} have attributed the rather high melting point of BH₃NH₃ to an attractive B–H···H–N interaction dubbed the “dihydrogen bond”.³³ What follows is a deuterium NMR spectroscopic study of solid BD₃NH₃ and BH₃ND₃. Our goal is to gain some insight into the strengths of the intermolecular interactions in solid BH₃NH₃ by measuring the deuterium quadrupolar coupling constants $\chi(\text{BD})$ and $\chi(\text{ND})$, the rotational correlation times, τ_c , and Arrhenius activation energies, E_a , for the rotation of the selectively deuterated BD₃ and ND₃ moieties. The phase dependence of the structure and NMR parameters for BH₃NH₃ and related compounds is the subject of a separate study.³⁵

Theoretical Background

Line Shapes. The solid-state deuterium NMR spectral line shape is dominated by the quadrupolar interaction. This is the interaction between the nuclear quadrupole moment, eQ , and the largest component of the electric field gradient (efg) tensor at the nucleus, eq_{zz} . The quadrupolar coupling constant, χ , which is a measure of the strength of the quadrupolar interaction is given as

$$\chi = \frac{e^2 q_{zz} Q}{h} \quad (1)$$

The line shape is also influenced by the asymmetry parameter of the efg tensor, η , which is defined as the difference between the two smaller principal components of the diagonalized electric field gradient tensor, eq_{xx} and eq_{yy} , with respect to the largest component, eq_{zz} :

$$\eta = \frac{eq_{xx} - eq_{yy}}{eq_{zz}} \quad (2)$$

For the molecule studied here, the η values are very small (<0.1) and it will be assumed that the efg is axially symmetric along the X–D bond. In that case, the spectrum from a deuterium nucleus located in a static X–D bond consists of a doublet with spacing

$$\Delta\nu = \frac{3e^2 q_{zz} Q}{4h} (3 \cos^2 \alpha - 1) \quad (3)$$

where α is the angle between the X–D bond and the static magnetic field, B_0 . For powdered samples, the line shape is determined by the random distribution of the X–D bond orientations with respect to B_0 , yielding a typical Pake doublet with a characteristic splitting between peaks ($\alpha = 90^\circ$) of $3\chi/4$ and shoulders ($\alpha = 0^\circ$) separated by $3\chi/2$. See Figure 1. The effects of motion on the deuterium powder spectrum are 2-fold. First, the width of the spectral line is narrowed by the motion. In the case of a jumping motion of the X–D bond between three or more equally populated sites, as is expected for ND₃ and BD₃ groups, η is averaged to zero and, if the motion is fast compared to the quadrupolar interaction (i.e., $>10^6 \text{ s}^{-1}$), the

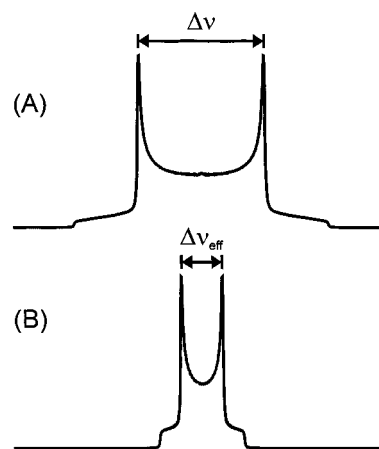


Figure 1. Simulated deuterium NMR spectra for (A) a static deuterium and (B) a deuterium undergoing three-site exchange.

quadrupolar splitting, $\Delta\nu$, is reduced to

$$\Delta\nu_{\text{eff}} = \frac{3\chi^2}{8} (3 \cos^2 \theta - 1) \quad (4)$$

where θ is the angle between the X–D bond and the rotational axis. If the motional rate, k , is of the order of χ ($\sim 10^4$ – 10^6 s^{-1}), the spectral line shape is severely distorted due to the large T_2 anisotropy associated with the dynamic process.³⁶ The distorted line shapes can readily be simulated for a given combination of χ , θ , and k .³⁷

Relaxation Times. The spin–lattice relaxation time, T_1 , characterizes the return of the bulk magnetization to its equilibrium state after a perturbing pulse. Relaxation is stimulated by time-dependent nuclear spin interactions and is most efficient when these fluctuations occur at the resonance frequency of the nucleus. For deuterons, the primary source of these fluctuating fields is the time-dependent part of the quadrupolar interaction.

When the reorientational motion can be described by an exponential correlation function and the temperature dependence of the correlation time follows Arrhenius behavior, the rate of relaxation may be fit to the following equations:³⁸

$$\frac{1}{T_1} = K \left(\frac{\tau_c}{1 + \omega_0^2 \tau_c^2} + \frac{4\tau_c}{1 + 4\omega_0^2 \tau_c^2} \right) \quad (5)$$

$$\tau_c = \tau_\infty \exp\left(\frac{E_a}{RT}\right) \quad (6)$$

where τ_c is the correlation time for the motion ($\tau_c \propto k^{-1}$), τ_∞ is its value at infinite temperature, and ω_0 is the Larmor precession frequency. In addition, E_a is the activation energy for the motion influencing T_1 , and K depends on the strength of the dominant nuclear spin interaction (in this case χ^2) and the exact nature of the reorientational motion. For jumps of the X–D bond among three or more equivalent positions oriented at an angle θ about the rotational axis, K is given by

$$K = \frac{9\pi^2 \chi^2}{20} (3 \cos^2 \theta - 1) \quad (7)$$

(33) Crabtree, R. H.; Siegbahn, P. E. M.; Eisenstein, O.; Rheingold, A. L.; Koetzle, T. F. *Acc. Chem. Res.* **1996**, *29*, 348.

(34) Richardson, T. B.; deGala, S.; Crabtree, R. H.; Siegbahn, P. E. M. *J. Am. Chem. Soc.* **1995**, *117*, 12875.

(35) Penner, G. H.; Chang, P.; Hutzal, J.; Grandin, H. M. Unpublished results.

(36) Hoatson, G. L.; Vold, R. L. In *Solid State NMR III: Organic Matter*; Blülich, B., Ed.; Springer-Verlag: New York, 1994.

(37) Greenfield, M. S.; Ronemus, A. D.; Vold, R. L.; Vold, R. R.; Ellis, P. D.; Raidy, T. R. *J. Magn. Reson.* **1987**, *72*, 89.

(38) Torchia, D. A.; Szabo, A. J. *Magn. Reson.* **1982**, *49*, 107.

In this case, if a plot of $\ln(T_1)$ vs inverse temperature is made, one often sees a V-shaped curve, with a T_1 minimum at $\omega_0\tau_c = 0.62$. There is, in general, much information to be extracted from this T_1 plot. The slope of the curve on either side of the T_1 minimum is characteristic of the activation energy for the motion influencing T_1 . The intercept at $1/T = 0$ yields a value for τ_∞ , while the depth of the minimum can be used to determine a value for the effective quadrupolar coupling constant. Note that knowledge of τ_∞ and E_a allows calculation of the motional rate at any temperature, through eq 6.

Experimental Section

A sample of BH_3ND_3 was prepared by the dissolving 1 g of $\text{BH}_3\text{-NH}_3$ (Aldrich) in 20 mL of D_2O and stripping off the D_2O under vacuum. A sample of BD_3NH_3 was prepared by the method of Hu, Van Paasschen, and Geanangel:³⁹ A 1.266 g sample of NaBD_4 and 3.258 g of $(\text{NH}_4)_2\text{CO}_3$ were added to 50 mL of dry THF, and the mixture was heated with stirring to 40 °C for 24 h. The resulting mixture was diluted with more THF and filtered, and the THF was removed by evaporation under vacuum. Sample purities were checked by ^{11}B and ^{14}N high-resolution NMR spectroscopy in aqueous solution. No impurity peaks could be found in these spectra. About 100-mg samples were packed into standard 5 mm o.d. NMR tubes which had been cut to a length of 3 cm.

The deuterium spectra were recorded on a Bruker ASX-200 NMR spectrometer operating at 30.7 MHz, using the quadrupolar echo pulse sequence: $(\pi/2)_x - \tau_Q - (\pi/2)_y - \tau_Q - \text{acquire}$.⁴⁰ The length of the $\pi/2$ pulse was approximately 2.5 μs . At each temperature, the echo signals were collected for a τ_Q value of 40 μs . The echo signals were Fourier transformed to obtain the deuterium NMR spectra. The temperature of the sample chamber was electronically regulated by a Eurotherm B-VT 2000 temperature controller to within ± 0.2 °C over the course of a measurement. The true temperature of the sample was recorded just prior to each measurement by lowering a copper-constantan thermocouple down the gas venting tube until it came into contact with the sample coil. The estimated uncertainty of the recorded sample temperature was about ± 0.5 °C.

The deuterium T_1 data were acquired using an inversion recovery pulse sequence modified for quadrupolar nuclei: $(\pi)_x - \tau - (\pi/2)_{\pm x} - \tau_Q - (\pi/2)_y - \tau_Q - \text{acquire}$.⁴¹ Typically, 12 values of τ were used to determine T_1 at each temperature. The pulse spacing, τ_Q , for the T_1 determination was 40 μs . The time between repetitions of the pulse sequence was always greater than $5T_1$. The data were fit using a nonlinear least-squares algorithm employing an exponential fitting function to obtain the relevant relaxation time parameters.

Quadrupolar echo spectra were simulated by standard methods using the program MXQET.³⁷ Simulated spectra were visually matched to experimental line shapes. The T_1 data were least-squares-fit to the BPP spectral density function, to obtain the activation energy, E_a , the correlation time at infinite temperature, τ_∞ , and the effective quadrupolar coupling constant, χ_{eff} .

Molecular orbital calculations were performed using Gaussian 94⁴² on a 300 MHz Pentium II personal computer. The deuterium χ values (in MHz) were obtained from the computed efg values (in atomic units)

(39) Hu, M. G.; Van Paasschen, J. M.; Geanangel, R. A. *J. Inorg. Nucl. Chem.* **1977**, *39*, 2147.

(40) Davis, D. H.; Jeffrey, K. R.; Bloom, M.; Valic, M. I.; Higgs, T. P. *Chem. Phys. Lett.* **1976**, *42*, 390.

(41) Demco, D. E.; van Hecke, P.; Waugh, J. S. *J. Magn. Reson.* **1974**, *16*, 467.

(42) Frisch, M. J.; Trucks, G. W.; Schlegel, H. B.; Gill, P. M. W.; Johnson, B. G.; Robb, M. A.; Cheeseman, J. R.; Keith, T. A.; Petersson, G. A.; Montgomery, J. A.; Raghavachari, K.; Al-Laham, M. A.; Zakrzewski, V. G.; Ortiz, J. V.; Foresman, J. B.; Cioslowski, J.; Stefanov, B. B.; Nanayakkara, A.; Challacombe, M.; Peng, C. Y.; Ayala, P. Y.; Chen, W.; Wong, M. W.; Andres, J. L.; Replogle, E. S.; Gomperts, R.; Martin, R. L.; Fox, D. J.; Binkley, J. S.; Defrees, D. J.; Baker, J.; Stewart, J. P.; Head-Gordon, M.; Gonzalez, C.; Pople, J. A. *Gaussian 94*, Revision D.3; Gaussian, Inc.: Pittsburgh, PA, 1995.

(43) Pyykkö, P. Z. *Naturforsch.*, **A 1992**, *47*, 189.

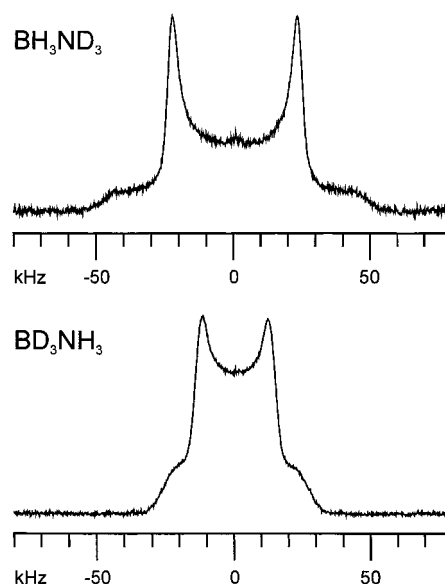


Figure 2. Deuterium NMR spectra of solid BD_3NH_3 and BH_3ND_3 at room temperature.

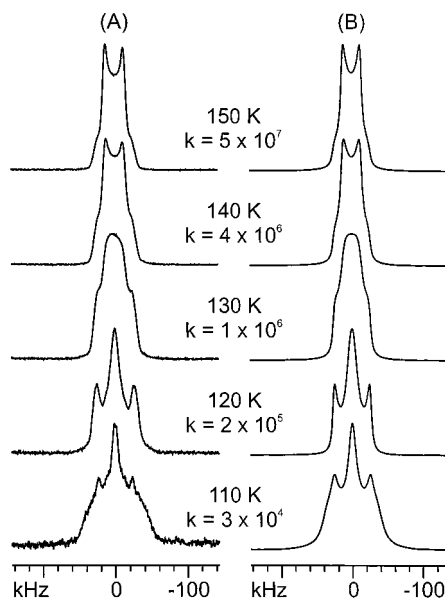


Figure 3. Deuterium spectra of solid BD_3NH_3 below 150 K together with simulations for different rates, k (in s^{-1}), of 3-fold rotation.

using the relationship $\chi = -237(eq_{zz})(eQ)$, where an eQ value of 2.86 barns (1 barn = 10^{-28} m^2) was used.⁴³

Results and Discussion

Deuterium Line Shapes. The deuterium spectra for $\text{BD}_3\text{-NH}_3$ and BH_3ND_3 at room temperature are shown in Figure 2. Using eq 4 and tetrahedral geometries at the boron and nitrogen, together with the assumption that the molecules are performing rapid n -site rotation, yields χ values of 105 ± 5 and 198 ± 5 kHz for the B–D and N–D deuterons, respectively.

The deuterium line shape of BH_3ND_3 does not change appreciably down to 116 K. The line shape for BD_3NH_3 does change below 150 K, and the spectra for BD_3NH_3 , together with simulations, are presented in Figure 3. Simulations of the temperature dependence of the deuterium spectra employed a three-site jump model and were carried out with three adjustable parameters: the exchange rate, k , the N–B–H bond angle, $180^\circ - \theta$, and the static (unaveraged) $\chi(\text{BD})$ value. The series of

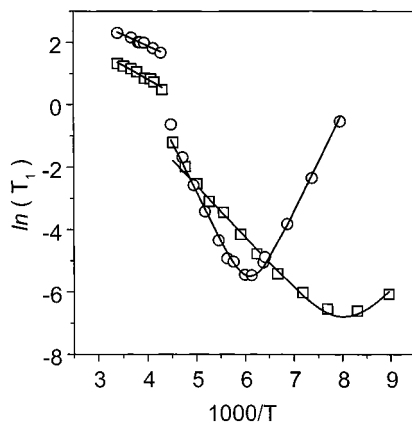


Figure 4. Temperature dependence of the deuterium T_1 (in s) for solid BD_3NH_3 (circles) and BH_3ND_3 (squares) between 115 and 300 K.

spectra were best fit with a θ value of $70.5 \pm 2^\circ$ and a $\chi(\text{BD})$ of 105 ± 10 kHz. The best rate at each temperature is shown in Figure 3. A considerable amount of line broadening had to be included in the simulations due to the rather large $^{11}\text{B}-^2\text{H}$ dipolar couplings, $D(^{11}\text{B}, ^2\text{H})$. For example the value of D , unaveraged by the 3-fold rotation, is 3.3 kHz per B–D bond. A fit of the temperature-dependent rates to the Arrhenius equation yields an activation energy, E_a , of 25 ± 2 kJ/mol and a preexponential factor, A , of $7.0 \times 10^{17} \text{ s}^{-1}$.

Spin–Lattice Relaxation Times. The temperature dependence of the deuterium T_1 for BD_3NH_3 and BH_3ND_3 between about 115 and 300 K is shown in Figure 4. Solid BH_3NH_3 undergoes a phase transition at about 220 K, between a low-temperature orthorhombic phase and a high-temperature tetragonal phase.^{8,10} This phase transition can be seen clearly as breaks in the T_1 curves. No attempt was made to determine accurately the phase transition temperature. The slopes of the $\ln T_1$ versus $1/T$ curves above 220 K yield E_a values of 5.9 ± 0.5 and 7.3 ± 0.8 kJ/mol for BD_3NH_3 and BH_3ND_3 , respectively. Below the phase transition, each of the T_1 curves passes through a minimum. These curves can be fit to eqs 5 and 6. If a tetrahedral geometry is assumed ($\theta = 70.5^\circ$), the factor K in eq 5 becomes $3\pi^2/10$ and the resulting fits yield $\chi = 105 \pm 5$ kHz, $\tau_\infty = 1.2 \times 10^{-17}$ s, and $E_a = 26.4 \pm 1.4$ kJ/mol for the deuterons in BD_3NH_3 and $\chi = 202 \pm 5$ kHz, $\tau_\infty = 5.7 \times 10^{-15}$ s, and $E_a = 13.7 \pm 0.9$ kJ/mol for the deuterons in BH_3ND_3 . The χ values are in good agreement with those obtained from the spectral line shapes. The E_a value for BD_3 rotation is also in good agreement with that obtained from the temperature dependence of the line shapes in BD_3NH_3 . The value of A from the line shape analysis yields $\tau_\infty = 4.7 \times 10^{-19}$ s, in poor agreement with the T_1 results. This is not surprising since the two values result from rather extended extrapolations to $1/T = 0$ and the slope from the line shape study has a relatively large error associated with it. Although the T_1 minima are not observed in the high-temperature phase, the values of τ_∞ can be estimated from the activation energy and an extrapolation of the $\ln T_1$ versus $1/T$ curve into the orthorhombic phase. Since the ^2H T_1 minimum occurs at $\omega_0\tau_c = 0.62$, $\tau_\infty(\text{BD})$ and $\tau_\infty(\text{ND})$ values of 1.1×10^{-13} and 4.4×10^{-14} s are obtained respectively. The best way to compare the motions of the BD_3 and ND_3 groups is to consider the rotational correlation times as obtained from the deuterium T_1 measurements. The temperature dependencies of $\tau_c(\text{BD})$, for the BD_3 group in solid BD_3NH_3 , and of $\tau_c(\text{ND})$, for the ND_3 group in solid BH_3ND_3 , are shown in Figure 5. For an exchange between n equivalent sites, $\tau_c = 1/(nk)$, where k is the exchange rate constant. Figure 5

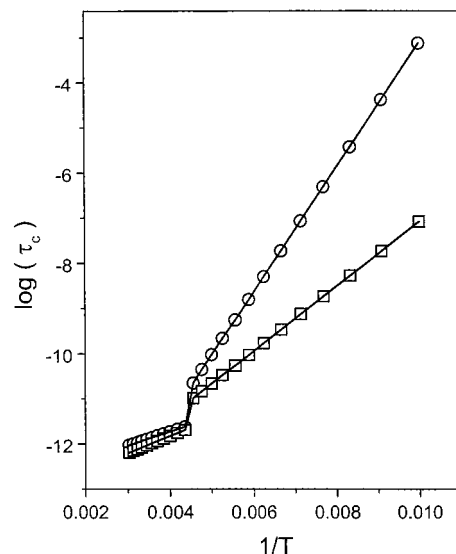


Figure 5. Rotational correlation times for the BD_3 group in BD_3NH_3 , $\tau_c(\text{BD})$ (circles), and for the ND_3 group in BH_3ND_3 , $\tau_c(\text{ND})$ (squares).

Table 1. Sensitivity of $\chi(\text{BD})$ and $\chi(\text{ND})$ to Changes in the Structure of BH_3NH_3^a

	$\chi(\text{BD})$ (kHz)	$\chi(\text{ND})$ (kHz)	$\chi(\text{BD})$ (kHz)	$\chi(\text{ND})$ (kHz)
r_{BN} {	135	257	136	260
1.5 Å	136	260		
r_{BH} {	147	260	136	259
1.20 Å	133	260		
r_{NH} {	136	285	136	260
1.02 Å	136	249		

^a Bond lengths and bond angles were chosen to bracket the measured gas-phase microwave values; all other parameters were held at latter values.

provides two important pieces of information. First, the two correlation times are equal, within experimental uncertainty, in the high-temperature phase (above 220 K). The internal rotational barrier in isolated BH_3NH_3 is 8.5 ± 0.1 kJ/mol.⁴ This is larger than the E_a values for BD_3 and ND_3 rotation obtained from our T_1 studies in the solid state. We calculate a barrier of 9.3 kJ/mol at the MP2/6-31G(d,p) level using the gas-phase B–N bond length of 1.672 Å. If the solid-state bond length of 1.564 Å is used, the barrier increases significantly to 12.8 kJ/mol. It is therefore reasonable to conclude that, in the high-temperature phase, the BD_3 and ND_3 groups are rotating together to yield an overall BH_3NH_3 molecular reorientation with a rather low activation energy (< 8 kJ/mol). This is also the case for CH_3NH_3^+ in the high-temperature solid phase of $(\text{CH}_3\text{NH}_3)_2\text{TeCl}_6$.⁴⁴ Second, in the low-temperature phase, $\tau_c(\text{BD})$ and $\tau_c(\text{ND})$ differ increasingly as the temperature is lowered. The correlation time for the ND_3 deuterons increases more rapidly with lower temperature. In other words, the ND_3 rotation slows down more with a decrease in temperature than the BD_3 rotation. The work of Reynhardt and Hoon¹⁰ relies mainly on the ^1H T_1 of BH_3NH_3 as a function of temperature. A comparison of our results and those of Reynhardt and Hoon is provided in Table 1. As the ^1H T_1 in the high-temperature phase is dominated by reorientation of the BH_3 protons, these authors were unable to determine activation parameters for the NH_3 rotation in this phase. In the low-temperature phase, the ^1H T_1 measurements exhibit nonexponential behavior. Reynhardt and Hoon fit the experimental magnetization curves to a biexponential function, yielding short T_1 and long T_1 components. This results in a

significant scatter in the $\ln T_1$ versus $1/T$ curve and complicates the analysis. Despite this, there is reasonably good agreement between our results and those of Reynhardt and Hoon. The advantage of selective deuteration is that the motions of the BD_3 and ND_3 groups can be followed separately via the deuterium NMR relaxation times. In addition, there is no complicating nonexponential behavior when the total magnetization is considered as a function of the delay, τ . Third, the BD_3 and ND_3 spectral changes can be followed separately and simulated, whereas the ^1H spectrum is due to both the BH_3 and NH_3 protons and shows nearly featureless line shapes.

One thing that the line shape and T_1 measurements do not directly tell us is the "foldedness" of the potential barriers hindering BD_3 and ND_3 rotation. Here one must rely on crystallographic information. Although single crystals of $\text{BH}_3\text{-NH}_3$ suitable for diffraction studies have never been successfully grown, a thorough variable-temperature powder diffraction investigation has been reported by Hoon and Reynhardt.¹⁰ In the high-temperature tetragonal phase, each hydrogen atom can occupy any of 12 equivalent positions. Therefore, it is reasonable to assume that the rotational barrier is 12-fold in the tetragonal phase. Similarly, the hydrogens can occupy three sites in the low-temperature orthorhombic phase, yielding a 3-fold barrier. If equally populated sites are assumed, the rotational potential energy function will have the form

$$V(\theta) = V_n \sin^2\left(\frac{n\theta}{2}\right) \quad (8)$$

where V_n is the height of the n -fold barrier.

One way of looking into the foldedness of the ND_3 and BD_3 rotation is through the anisotropy in T_1 . This anisotropy results in an unequal rate of recovery of the magnetization across the powder spectrum after an rf pulse. The anisotropy is due to the dependence of T_1 on the orientation of the X–D bond with respect to the applied magnetic field. Torchia and Szabo³⁸ have developed a formalism by which the T_1 anisotropy can be related to the dynamics of the X–D bond. In general, for simple exchange among three or more equivalent sites, the shoulder intensity recovers more rapidly than that of the peaks. An important result of the work of Torchia and Szabo and others^{38,45} is that the T_1 anisotropy disappears if n is very large or if V_n is very small, that is, for diffusive motion, as opposed to discrete n -site jumps. Therefore, we expect to observe T_1 anisotropy in the inversion recovery spectra below 220 K but much less above this temperature. Line shapes for fully inverted spectra and the null point are shown in Figure 6. At 200 K, the ^2H inversion recovery experiments show T_1 anisotropy for BD_3NH_3 and $\text{BH}_3\text{-ND}_3$. At 290 K, a smaller T_1 anisotropy is observed for $\text{BD}_3\text{-NH}_3$ and no anisotropy is observed for BH_3ND_3 . These are the expected results.

Deuterium Quadrupolar Coupling Constants. In principle, the deuterium QCCs should provide information about the electronic structure in the proximity of the hydrogen of interest. It is probably best to start by investigating the sensitivity of $\chi(\text{BD})$ and $\chi(\text{ND})$ to the various structural parameters of $\text{BH}_3\text{-NH}_3$. The calculated effects of r_{BN} , r_{BH} , r_{NH} , θ_{NBH} , and θ_{BNH} are presented in Table 1. As can be seen, $\chi(\text{XD})$ is significantly more sensitive to changes in the X–D bond length than for any other parameter. This is in line with the generally accepted idea that nuclear quadrupolar coupling constants probe local

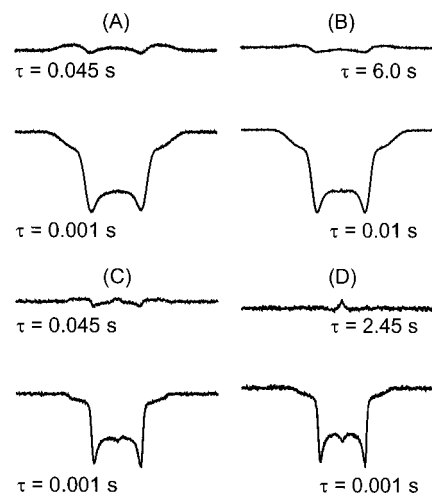


Figure 6. Fully inverted and null-point deuterium inversion recovery spectra: (A) BD_3NH_3 at 200 K; (B) BD_3NH_3 at 290 K; (C) BH_3ND_3 at 200 K; (D) BH_3ND_3 at 290 K.

electronic structure.⁴⁶ It is rather unfortunate that, at this time, an accurate molecular structure of solid BH_3NH_3 is not available. The best we can do at present is to perform a geometry optimization on BH_3NH_3 with a fixed bond length of 1.564 Å (the accepted solid-state value)³² and calculate $\chi(\text{BD})$ and $\chi(\text{ND})$ for an isolated molecule. The values calculated at the CI-(SD)/6-31G(d,p) level after optimization of all other geometric parameters at the MP2/6-31G(d,p) level ($r_{\text{BH}} = 1.206$ Å, $r_{\text{NH}} = 1.016$ Å, $\theta_{\text{BNH}} = 111.6^\circ$, and $\theta_{\text{NBH}} = 105.4^\circ$) are 143 and 255 kHz, respectively. These are significantly larger than our measured values. It should be pointed out that, with the exception of the line shape study of BD_3NH_3 , our analyses assumed a tetrahedral geometry for both the BD_3 and ND_3 groups. This is different from the geometry calculated above and the gas-phase microwave values of $\theta_{\text{NBH}} = 104.7^\circ$ and $\theta_{\text{BNH}} = 110.3^\circ$. If, for example, the gas-phase microwave geometry were used instead of the ideal geometry, the values of $\chi(\text{BD})$ and $\chi(\text{ND})$ would decrease and increase, respectively, to 87 and 209 kHz. These values are still significantly smaller than the those calculated for an isolated molecule. It is interesting to note that $\chi(\text{CD})$ values for such molecules as benzene and chloroform change very little between the gas and condensed phases.⁴⁷ On the other hand, $\chi(\text{ND})$ is expected to change (decrease) significantly if hydrogen bonding is expected in the condensed phase. For example Laaksonen and Wasylischen⁴⁸ have suggested values of about 265 and 190 kHz for ND_3 in the gas and solid phases, respectively. We calculate values of 277 and 201 kHz (CI-(SD)/6-31G(d,p)) using the gas- and solid-phase molecular structures of ND_3 . The crystal structure of solid ND_3 shows an elongation of the N–D bond, presumably due to intermolecular hydrogen bonding. We have measured $\chi(\text{ND})$ values of 162 ± 5 kHz in zwitterionic ND_3SO_3 and 184 ± 5 kHz in ND_3BF_3 .⁴⁹ In these solids, N–H \cdots O or N–H \cdots F intermolecular hydrogen bonding is expected.

Conclusion

The activation energies and τ_∞ values for BD_3NH_3 and $\text{BH}_3\text{-ND}_3$ in the high- and low-temperature phases, together with the results of Hoon and Reynhardt, are shown in Table 2. In the

(46) Bailey, W. C. *J. Mol. Spectrosc.* **1998**, *190*, 318.

(47) Butler, L. G.; Keiter, E. A. *J. Coord. Chem.* **1994**, *80*, 121.

(48) Laaksonen, A.; Wasylischen, R. E. *Z. Naturforsch., A* **1995**, *50*, 137.

(49) Penner, G. H.; Chang, P.; Grandin, H. M.; Reynolds, J. Unpublished results.

(44) MacIntosh, M. R.; Gruwel, M. L. H.; Robertson, K. N.; Wasylischen, R. E. *Can. J. Chem.* **1992**, *70*, 849.

(45) Wittebort, R. J.; Olejniczak, E. T.; Griffen, R. G. *J. Chem. Phys.* **1987**, *86*, 5411.

Table 2. Activation Energies and Correlation Times for BD_3 and ND_3 Rotation in Solid BD_3NH_3 and BH_3ND_3

phase	group		E_a (kJ/mol)	τ_∞ (s)
high temp (tetragonal)	BD_3	<i>a</i>	5.9 ± 0.5	1.1×10^{-13}
		<i>b</i>	5.9 ± 0.4	1.2×10^{-14}
	ND_3	<i>a</i>	7.3 ± 0.8	4.4×10^{-14}
low temp (orthorhombic)	BD_3	<i>b</i>	N/A	N/A
		<i>a</i>	25.4 ± 1.4	1.2×10^{-17}
		<i>b</i>	25 ± 0.4	6.7×10^{-18}
	ND_3	<i>c</i>	24.3 ± 1.9	4.3×10^{-17}
		<i>a</i>	13.7 ± 0.9	5.7×10^{-15}
	<i>b</i>	9.6 ± 0.4	9.5×10^{-14}	

^a Present work; deuterium T_1 . ^b Reference 11; proton T_1 . ^c Present work; deuterium line shapes.

high-temperature phase, the activation energies for BD_3 and ND_3 rotation are smaller than that for internal rotation and correlation times for BD_3 and NH_3 are close enough to consider the possibility of the reorientational motion as being a whole molecule reorientation about the B–N bond. In the low-temperature phase, the two motions are independent, in agree-

ment with the earlier proton NMR study of Hoon and Reynhardt. In this phase, the T_1 anisotropy experiments are consistent with 3-fold rotational potentials. In the high-temperature phase, the ND_3 deuterons show no T_1 anisotropy and the BD_3 deuterons show diminished anisotropy. The latter observation is consistent with the predicted 12-fold rotational potential and a smaller barrier height in the high-temperature phase.

Our measured deuterium quadrupolar coupling constants are significantly smaller than those we calculate at reasonably high levels of molecular orbital theory. This is possibly due to a slight lengthening of the B–H and N–H bonds, a result of attractive B–H···H–N interactions. A definite answer to this problem requires the determination of the gas-phase deuterium quadrupolar coupling constants for BD_3NH_3 and BH_3ND_3 and high-level calculations of these coupling constants on an accurate (neutron diffraction) solid-state structure.

Acknowledgment. We thank the Natural Sciences and Engineering Research Council of Canada for financial support.

IC981370F